Assessment of Land Surface Changes in the Vicinity of Underground Gas Storage Using Multispectral Remote Sensing

Aleksandra Kaczmarek[1], Jan Blachowski[1]

[1] Department of Geodesy and Geoinformatics, Faculty of Geoengineering, Mining and Geology, Wrocław University of Science and Technology, Wybrzeże Stanisława Wyspiańskiego 27, 50-370 Wrocław, Poland - (aleksandra.kaczmarek, jan.blachowski)@pwr.edu.pl

Keywords: Sentinel-2, Vegetation, Water Detection, Spatial Statistics.

Abstract

Geological formations are used worldwide for storage of energy sources and carriers such as natural gas and hydrogen, but also carbon dioxide. Caverns in rock salt are a specific type as due to the properties of salt, they are particularly suitable for long term safe and stable storage of various materials. However, the operation interacts with the environment in several ways, with ground movements being the most observed. The purpose of this study was to analyse land cover changes in the vicinity of underground gas storage based on a case study area of Kosakowo, Poland. The region is mainly agricultural with a neglected drainage system, located close to the sea, at low altitude, making it prone to waterlogging. The condition and changes in land surface, with vegetation and surface water monitoring in particular, were analysed using spectral indices derived from the ESA Copernicus Sentinel-2 data. In the study, it was tested and validated whether and if open multispectral satellite data in connection with spatial statistics can be effectively used for monitoring land cover changes in such regions.

1. Introduction

Underground gas storage (UGS) is an element of the energy sector aimed at maintaining the reserves during low and high-demand periods throughout the year. It is commonly used for storage of hydrocarbons and, increasingly, hydrogen. Geological storage projects are created in various formations, including depleted oil and gas reservoirs, aquifers and porous media, or rock caverns. The latter are mainly developed in salt deposits, as due to the unique properties of rock salt, it is particularly suitable for storage, ensuring long-term stability and safety (Liu et al., 2023). Underground gas storage (UGS) interacts with the environment in a number of ways. The main impact observed on the surface is the subsidence caused by the cavern convergence. The subsidence can be superimposed with cyclical movements caused by pressure changes inside the caverns (Tarkowski et al., 2024). As salt is a plastic medium, the effects of salt mining on the surface appear with a temporal delay and are observed decades after mine closure. However, the characteristics of UGS operations differ, as gas is alternately injected into and withdrawn from storage caverns, causing cyclical upward and downward movements of the land surface (Benetatos et al., 2020). Combined with shallow groundwater level or intense rainfall events that have become more frequent in recent years due to climate change (Dong and Sutton, 2025), it can cause local waterlogging and flooding, affecting the vegetation condition.

Monitoring in geological storage sites includes a collection of methods providing complex analysis of the storage infrastructure and its surroundings. Land surface changes are evaluated using geodetic measurements of ground displacements such as precise levelling, which provide high quality of measurement (mm accuracy). However, the data are limited in time and space. Synthetic aperture radar (SAR) interferometry provides an alternative to classical geodetic approaches by offering frequent monitoring of large areas. It has been successfully applied in areas of underground storage for monitoring subsidence and seasonal movements associated with operation phases (Fibbi et al., 2023; Struhár et al., 2022; Zhang et al., 2022). SAR data can also be used in environmental studies of soil moisture (Guo et al., 2019) or seasonal land cover changes (Czarnogorska et al., 2016). Their main advantage over passive remote sensing is the independence from weather conditions and clouds. Multispectral imagery is proven to be efficient in monitoring earth surface and changes that could be applied to UGS sites such as monitoring of peats and wetlands (Räsänen et al., 2022), waterlogging (Han et al., 2024), or surface water dynamics (Yang et al., 2020).).

The purpose of this work is to test and validate if open multispectral satellite data in connection with spatial statistics functions can be effectively used for monitoring land cover changes in underground gas storage sites with vegetation condition and waterlogging phenomena in particular focus. Selected spatial statistics methods were applied to process and analyse multispectral satellite imagery to identify areas of statistically significant changes in the time and space domains.

2. Materials and Methods

2.1 Study Area

The study area represents an underground gas storage facility in northern Poland at approximately 54°36'22'' N and 18°27'15'' E (Figure 1). It is located in close proximity to the Baltic Sea and the cities of Gdańsk and Gdynia. The site consists of 2 clusters of 5 caverns each constructed in the Mechelinki salt deposit at a depth of approx. 1000 m below the surface. The total capacity of the caverns is approx. 295.2 million m3.

The upper geological layers of the region are mainly of Quaternary and Holocene origin. The agricultural area located north of the UGS facility includes peats and shrublands. The thickness of the peat layer reaches up to 6 meters. Due to the low altitude, shallow groundwater level, proximity to the sea, and given geological conditions, the area is prone to waterlogging and local flooding.

https://doi.org/10.5194/isprs-archives-XLVIII-G-2025-749-2025

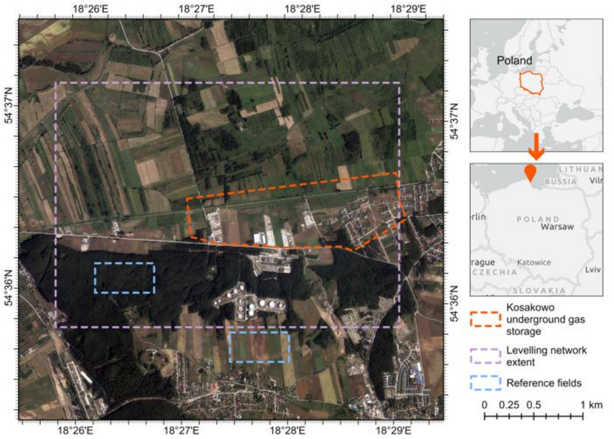

Figure 1. Location of the underground gas storage facility in Kosakowo, Poland.

For the purpose of this study, two study areas were identified. The first represents the area of the Kosakowo UGS legal permit, while the second corresponds to the extent of the monitoring network. The levelling network includes two measurement lines located perpendicularly to each other. Additionally, two reference fields were selected beyond the mining area of the UGS and peats. These represent crops and forests.

2.2 Data

The analysis was based on data acquired by the European Space Agency (ESA) Copernicus Sentinel-2 mission. The multispectral imagery at processing level 2A (L2A) was selected. The data are atmospherically corrected and represent surface reflectance. The L2A processing ensures a common radiometric scale and allows for multitemporal analysis and comparison (Song et al., 2001).

The data were accessed through Google Earth Engine Catalog and Copernicus Data Space Ecosystem. No initial cloud cover threshold was set, as for 10% and period 2015-2024 the data rejection rate was 90%. The images were selected manually to increase the amount of data and temporal coverage. In the analysis, 91 cloudless images acquired over the period 2014-2024 were used. 80 of them were acquired during the vegetation season from May to September.

2.3 Methods

As the area is primarily croplands and barren land with vegetation growing on peat, there are no in situ measurements of soil moisture or vegetation condition. Thus, the analysis was based on open-access satellite remote sensing data and Geographic Information System (GIS) processing tools employed in ArcGIS Pro software (ArcGIS Pro, 2024), Google Earth Engine (Gorelick et al., 2017) and Python language (Python, 2024).

2.3.1 Urban Area Mask: Bright built-up features in the images may be a source of potential interpretation errors, as they can be mistakenly taken as bare soil or surface water bodies (Ma et al., 2019). Thus, urban areas within the analysis region were masked. The mask was developed based on the CORINE Land Cover 2018 dataset (CORINE Land Cover 2018, 2020). The classification of land cover types in the study area is presented in Figure 2.

The mask included the following classes: (1) discontinuous urban fabric, (2) industrial or commercial units, (3) airports, (4) sport and leisure facilities, (5) sea and ocean.

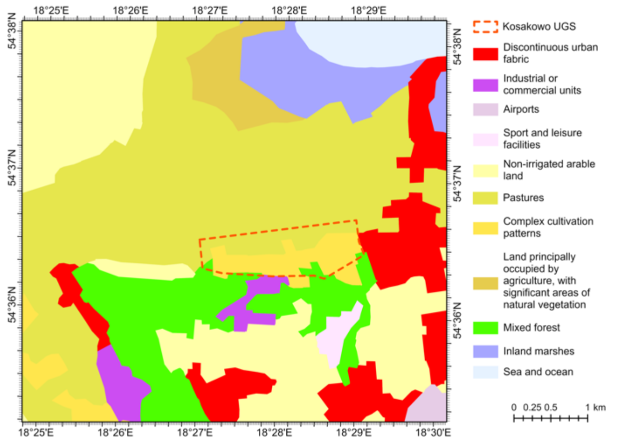

Figure 2. Land cover classification of the Kosakowo UGS region based on CORINE Land Cover 2018.

2.3.2 Spectral Indices: The images were aggregated into a multidimensional dataset allowing for simultaneous processing of data representing all time steps. For all images in the database, selected indices based on spectral reflectance were calculated for the assessment of vegetation, soil moisture and surface water. Water has moderate reflection in the visible light region (VIS) and strong absorption in short-wavelength infrared (SWIR). On the other hand, vegetation shows great absorption in the VIS region and reflection in near infrared (NIR). Plants with a high-water content tend to have low reflectance in SWIR. Thus, based on literature (McKenna et al., 2020; Sriwongsitanon et al., 2015) the following indices were selected for this study: normalized difference vegetation index (NDVI), normalized difference infrared index (NDII), and normalized difference water index (NDWI). The NDVI was proposed by Rouse et al. (1973) to monitor green vegetation vigour using spectral reflectance in the red and NIR regions.

$$NDVI = \frac{NIR - red}{NIR + red}, \tag{1}$$

where NIR = spectral reflectance in near infrared (840 nm)
red = spectral reflectance in red (665 nm)

The NDII (Hunt and Rock, 1989) is identical to the normalized difference moisture index (NDMI) (Gao et al., 1996). The index is used to describe the water content in plant canopies and, thus identify vegetation stress.

$$NDII = \frac{NIR - SWIR}{NIR + SWIR}, \tag{2}$$

where NIR = spectral reflectance in near infrared (840 nm)
$SWIR$ = spectral reflectance in short wavelength infrared (1610 nm)

The NDWI is used to delineate surface water bodies and monitor turbidity (McFeeters et al., 1996). The index allows the detection of flooded areas.

$$NDWI = \frac{green - NIR}{green + NIR}, \tag{3}$$

where *green* = spectral reflectance in green (560 nm)
NIR = spectral reflectance in near infrared (840 nm)

2.3.3 Spatiotemporal analysis: To analyse the variability in the time domain, a time series of the indices values was extracted to identify any patterns within the data. The processing was based on the concept of a space-time cube, where time is considered the third dimension (Figure 3).

Further, each pixel was processed separately to analyse its variation in time by calculating anomalies. An anomaly expresses the variation of a pixel value at a time with respect to the mean pixel value over a given time interval (ArcGIS Pro Documentation, 2024). In this study, it was computed as the difference from mean (Eq. 4) and z-score (Eq. 5). Z-score refers to the number of standard deviations in which the pixel value differs from the mean.

$$Difference\ from\ mean = x - \mu \tag{4}$$

$$Z - score = \frac{x - \mu}{s}, \tag{5}$$

where x = pixel value at a time slice
μ = mean of the pixel's values over a given time interval
S = standard deviation of the pixel's values over a given time interval

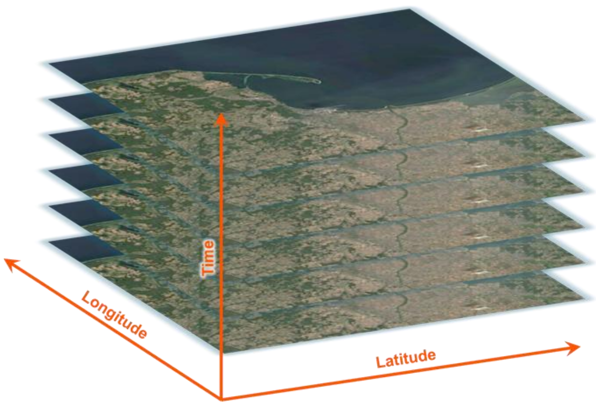

Figure 3. Visualisation of a multidimensional dataset of Sentinel-2 imagery.

The selected indices were further investigated spatially to analyse the distribution of the indices' values in space with the aim of identifying areas that undergo high temporal variability. It can be expressed through the coefficient of variation or through spatial clustering of pixels with similar values. Detection of clusters was carried out based on the concept of Getis-Ord Gi* statistic (Eq. 6-8) (Getis and Ord, 1992; Ord and Getis, 1995). Feature values are tested whether they are structured in complete spatial randomness. Based on the z-score and p-value, the pixels are assigned to clusters of statistically significant high or low values. Areas of high values are referred to as hot spots, while cold spots represent clusters of pixels with negative z-score.

$$G_i^* = \frac{\sum_{j=1}^{n} w_{ij} x_j - \underline{X} \sum_{j=1}^{n} w_{ij}}{S \sqrt{\frac{\left[n \sum_{j=1}^{n} w_{ij}^2 - \left(\sum_{j=1}^{n} w_{ij} \right)^2 \right]}{n-1}}}, \tag{6}$$

and

$$\underline{X} = \frac{\sum_{j=1}^{n} x_j}{n}, \tag{7}$$

$$S = \sqrt{\frac{\sum_{j=1}^{n} x_j^2}{2} - \left(\underline{X}\right)^2}, \tag{8}$$

where x = attribute value for feature j
w_{ij} = spatial weight between feature i and j
n = total number of features

The hot spot analysis can be applied to multidimensional datasets by evaluating the Gi* statistics using the Mann-Kendall test. The statistical test allows for detection of trends in time series data (Hamed, 2009).

3. Results

3.1 Time Series of Spectral Indices

Processing was based on more than 90 Sentinel-2 images that covered the area of interest. The time series plots of the indices exhibit seasonal changes related to the natural phenological cycle. Thus, the analysis was limited to images representing the vegetation period (Figures 4-6). To preserve short-term variability within the data, no temporal averaging was performed. Instead, representative images were selected for each month and year (Figure 7).

The spectral indices for vegetation monitoring follow the same patterns that exhibit seasonality throughout the vegetation period. The phenological cycle is also observed in the reference forest area. The high values of the NDVI, exceeding 0.5, indicate vigorous vegetation. The NDII at level 0.2-0.4 corresponds to a high canopy with a low level of water stress. On the other hand, the water index, NDWI, displays negative values indicating the absence of surface water. The two areas of interest represent structures more complex in land cover; thus, the indices values are overall lower. Moreover, the range of indices' values is wide, as the AOI is covered with crops, barren land, urban and industrial areas, or roads. The influence of urban, industrial areas and sea (east to the UGS facility) was limited by masking the features using CORINE Land Cover classes. However, the dataset has a spatial resolution of 100 m, and some smaller features may not be included.

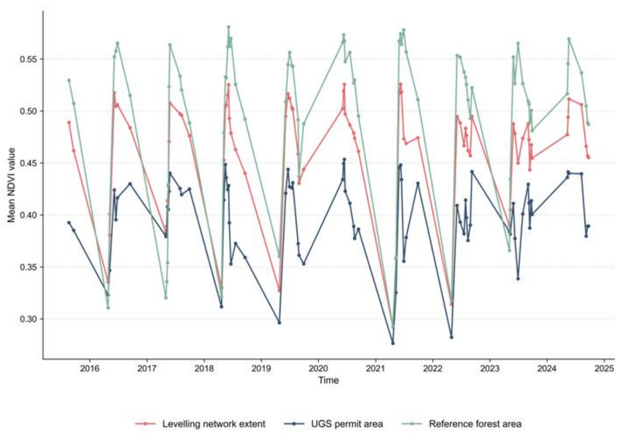

Figure 4. Time series of mean NDVI values in the Kosakowo UGS region.

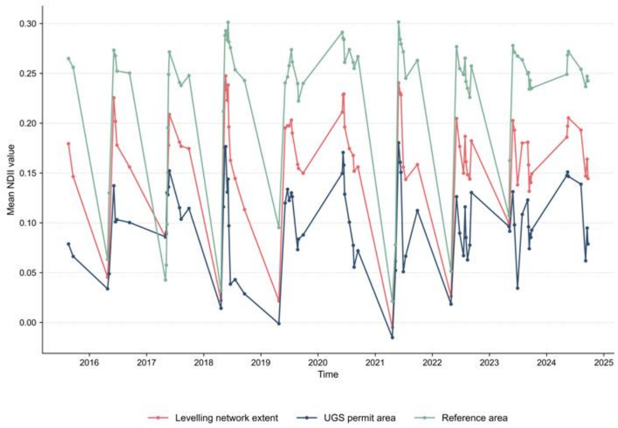

Figure 5. Time series of mean NDII values in the Kosakowo UGS region.

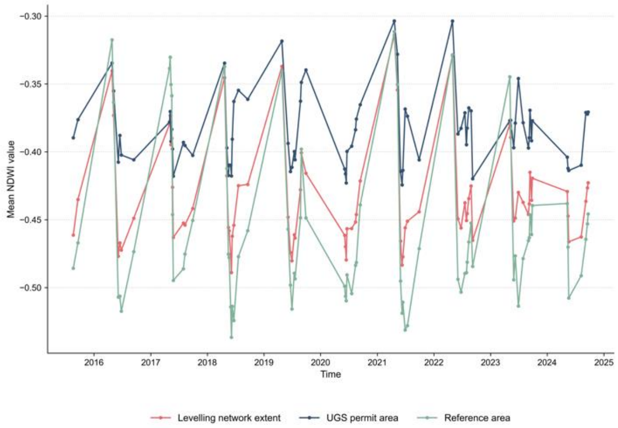

Figure 6. Time series of mean NDWI values in the Kosakowo UGS region.

The distribution of data is uneven in the time domain. Comparative analysis of images from a similar time period allows us to investigate long-term changes and patterns. However, it is prone to interpretation errors.

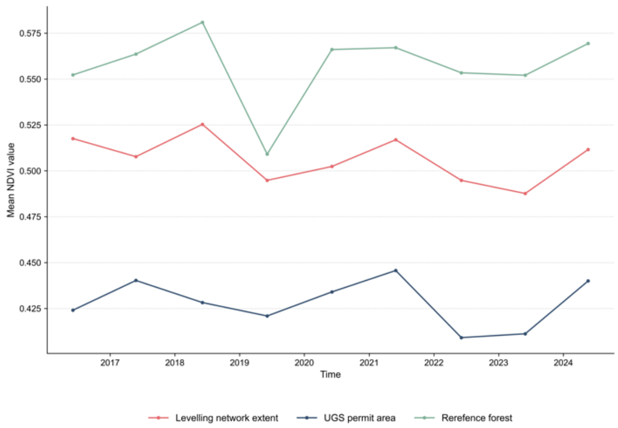

Figure 7. Time series of mean NDVI based on representative imagery from the turn of May and June.

The inverse response of the vegetation and water monitoring indices is reflected in the correlation coefficient, which is consistent throughout the study area (Figure 8).

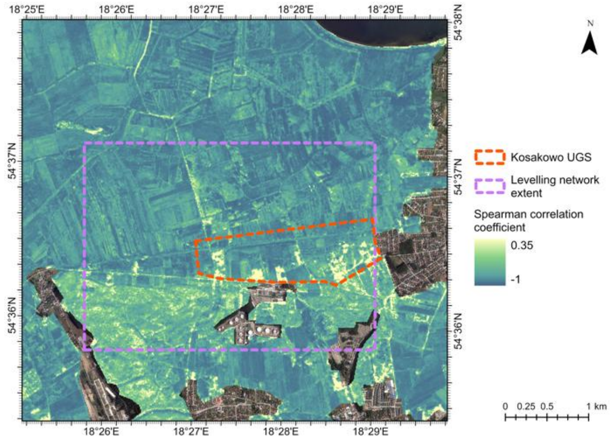

Figure 8. Correlation between the NDVI and NDWI values.

3.2 Anomaly Analysis

The anomalies were calculated based on 80 images with respect to the mean of all values. The majority of the area is covered with agricultural fields; therefore, the NDVI values exhibit positive variations from the mean (Figure 9). On the other hand, the NDWI values are negative, which is expected for such areas (Figure 10).

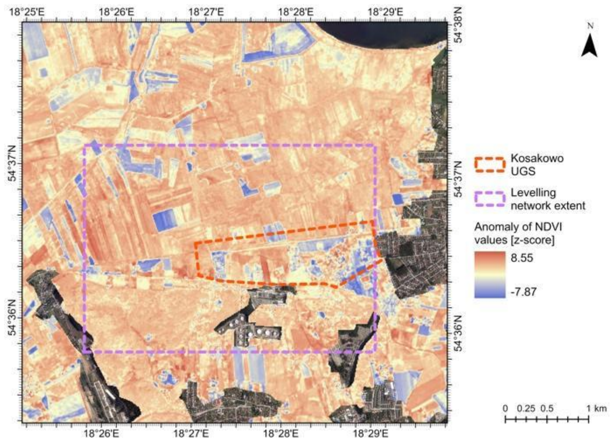

Figure 9. The anomaly of NDVI values expressed as z-score.

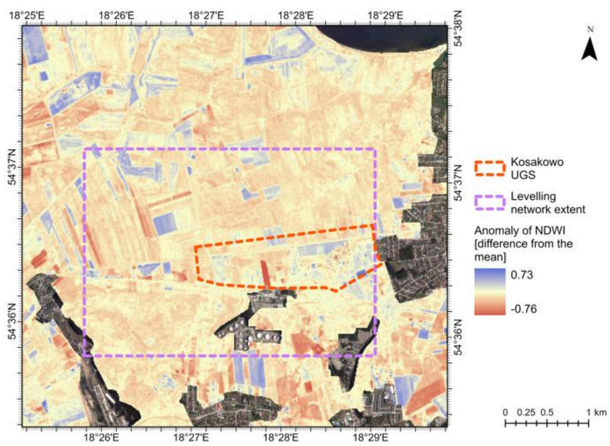

Figure 10. The anomaly of the NDWI values expressed as a difference from the mean.

Some fields located north-west of the UGS permit areas show different behaviour compared to the neighbourhood. The NDVI is lower than average, while the NDWI is high positive, which may indicate the temporal occurrence of water in the region. It is noteworthy that positive NDWI values are observed in the eastern part of the Kosakowo UGS area, but the pixels represent urban areas.

3.3 Hot Spot Analysis

Anomalies are based on a single pixel value change, while the hot spot analysis takes into consideration the behaviour of neighbouring pixels in both space and time domains. The temporal hot spots were determined considering the closest spatial neighbourhood of 20 m (Figure 11). Spatial autocorrelation plots, as well as temporal hot spot analysis based on the Getis and Ord statistic functions (Biwand and Wong, 2018), highlight areas that undergo frequent changes. In the case of the NDWI, most of the region is classified as an oscillating cold spot, meaning the pixels take negative values for most of the analysis period. There are also aggregations of statistically significant positive values. The clusters were identified mainly in the region located north-west of the UGS facility. The area is covered with crops and is of particular interest, as the area undergoes significant temporal variations of the spectral indices confirmed by a higher standard deviation compared to the reference area. The standard deviation of the indices for forest area is low and refers to the stable condition of the vegetation cover, which does not experience short-term changes. The appearance of the crop fields is of particular interest, as during the inspection of RGB images dark spots were discovered. They may indicate the periodic presence of surface water.

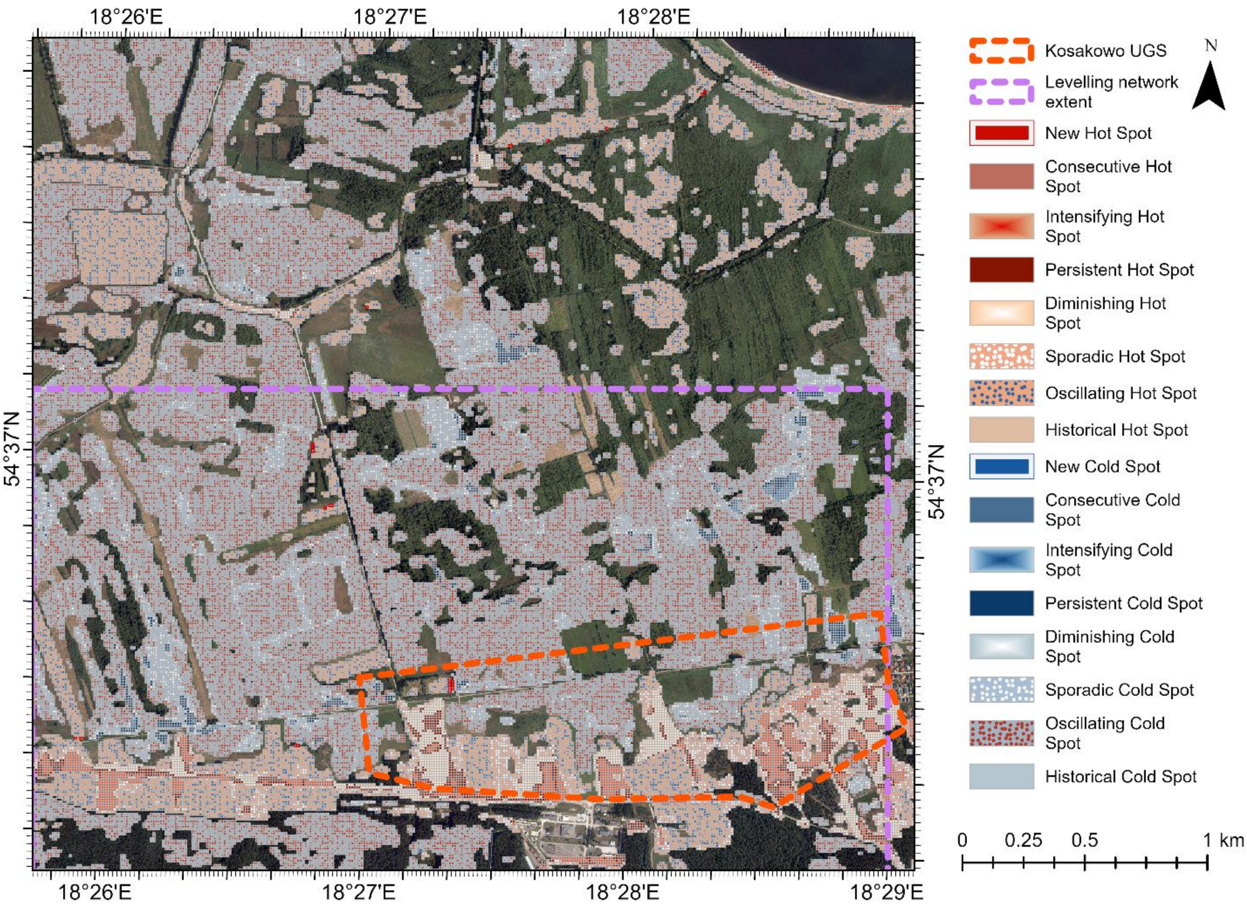

Figure 11. Temporal hot spots of the NDVI values in the Kosakowo UGS region.

4. Discussion and Conclusion

The presented preliminary results obtained for the case study indicate that this UGS region represents a complex environment that undergoes seasonal changes caused by the natural phonological cycle and meteorological conditions. The observed land cover changes may be an effect of the influence of peat layer and its changes in water content. Depending on the amount of water, peat may soak up the water from the rainfall or dry out during seasonal droughts, triggering changes in the land surface. The findings of our research show that detection of water using multispectral remote sensing poses many challenges, but periodic changes in the form of waterlogging can be studied through the analysis of vegetation condition with spatial statistics. The study presented an approach to analyse selected components of the environment above an underground gas storage facility using open access satellite imagery.

The results obtained in the preliminary study and the processes observed in the Kosakowo UGS are the subject of further analysis.

5. Acknowledgements

The work was carried out as part of the Closed-Loop Impact Monitoring for Environmentally and Socially Acceptable Energy

Transition in Rural Regions (acronym: CLEAR) project, supported by the National Centre for Research and Development, Poland [WPN/4/67/CLEAR/2022].

6. References

ArcGIS Pro, 2024. ArcGIS Pro software, Version 3.3.2. Esri Global Inc.

ArcGIS Pro Documentation, 2024. Generate Multidimensional Anomaly (Spatial Analyst). pro.arcgis.com/en/pro-app/latest/tool-reference/spatial-analyst/generate-multidimensional-anomaly.htm (12 December 2024)

Biwand, R.S., Wong, D.W.S., 2018. Comparing implementations of global and local indicators of spatial association. *Test*, 27, 716-748. doi.org/10.1007/s11749-018- 0599-x.

Benetatos, C., Codegone, G., Ferraro, C., Mantegazzi, A., Rocca, V., Tango, G., Trillo, F., 2020. Multidisciplinary Analysis of Ground Movements: An Underground Gas Storage Case Study. *Remote Sensing*, 12, 3487. doi.org/10.3390/rs12213487.

CORINE Land Cover 2018, 2020. European Union's Copernicus Land Monitoring Service information. doi.org/10.2909/71c95a07-e296-44fc-b22b-415f42acfdf0 (02 January 2025).

Czarnogorska, M., Samsonov, S.V., White, D.J., 2016. Airborne and Spaceborne Remote Sensing Characterization for Aquistore Carbon Capture and Storage Site, *Canadian Journal of Remote Sensing*, 42, 274–290. doi.org/10.1080/07038992.2016.1171131.

Dong, B., Sutton, R.T., 2024. Drivers and mechanisms contributing to excess warming in Europe during recent decades. npj *Climate and Atmospheric Science*, 8, 41. doi.org/10.1038/s41612-025-00930-3.

Fibbi, G., Beni, T., Fanti, R., Del Soldato, M., 2023. Underground Gas Storage Monitoring Using Free and Open Source InSAR Data: A Case Study from Yela (Spain), *Energies*, 16. doi.org/10.3390/en16176392.

Gao, B., 1996. NDWI - A normalized difference water index for remote sensing of vegetation liquid water from space. *Remote Sensing of Environment*, 58, 257–266. doi.org/10.1016/S0034-4257(96)00067-3.

Getis, A., Ord, J.K., 1992. The Analysis of Spatial Association by Use of Distance Statistics. *Geographical Analysis*, 24, 189–206. doi.org/10.1111/j.1538-46321992.tb00261.x.

Gorelick, N., Hancher, M., Dixon, M., Ilyushchenko, S., Thau, D., Moore, R., 2017. Google Earth Engine: Planetary-scale geospatial analysis for everyone. *Remote Sensing of Environment*, 202, 18-27. doi.org/10.1016/j.rse.2017.06.031.

Guo, S., Zheng, H., Yang, Y., Zhang, S., Hou, H., Zhu, Q., Du, P., 2019. Spatial estimates of surface deformation and topsoil moisture in operating CO2-EOR project: Pilot environmental monitoring using SAR technique, *Journal of Cleaner Production*. 236, 117606. doi.org/10.1016/j.jclepro.2019.117606.

Hamed, K.H., 2009. Exact distribution of the Mann–Kendall trend test statistic for persistent data. *Journal of Hydrology*, 365, 86–94. doi.org/10.1016/j.jhydrol.2008.11.024

Han F., Zhang X., Yu J., Xu S., Zhou G., Li S., 2024. Study on spatiotemporal dynamic characteristics of precipitation and causes of waterlogging based on a data-driven framework. *Science of The Total Environment*, 913, 169796. doi.org/10.1016/j.scitotenv.2023.169796

Hunt, E.R., Rock, B.N., 1989. Detection of changes in leaf water content using Near- and Middle-Infrared reflectances. *Remote Sensing of Environment*, 30, 43–54. doi.org/10.1016/0034-4257(89)90046-1.

Liu, W., Ding, W., Fan, J., Chen, J., Liu, W., Jiang, D., 2023. Creep properties and constitutive model of salt rocks under a slow cyclic loading path. *Journal of Energy Storage*, 72, 108761. doi.org/10.1016/j.est.2023.108761.

Ma, S., Zhou, Y., Gowda, P.H., Dong, J., Zhang, G., Kakani, V.G., Wagle, P., Chen, L., Flynn, K.C., Jiang, W., 2019. Application of the water-related spectral reflectance indices: A review. *Ecological Indicators*, 98, 68–79. doi.org/10.1016/j.ecolind.2018.10.049

McFeeters, S.K., 1996. The use of the Normalized Difference Water Index (NDWI) in the delineation of open water features. *International Journal of Remote Sensing*, 17, 1425–1432. doi.org/10.1080/01431169608948714.

McKenna, P.B., Lechner, A.M., Phinn, S., Erskine, P.D., 2020. Remote Sensing of Mine Site Rehabilitation for Ecological Outcomes: A Global Systematic Review. *Remote Sensing*, 12(21), 3535. doi.org/10.3390/rs12213535.

Ord, J.K., Getis, A., 1995. Local Spatial Autocorrelation Statistics: Distributional Issues and an Application. *Geographical Analysis*, 27, 286–306. doi.org/10.1111/j.1538-46321995.tb00912.x.

Python, 2024. Python, Version 3.12.2, Python Software Foundation.

Räsänen A., Tolvanen A., Kareksela S., 2022. Monitoring peatland water table depth with optical and radar satellite imagery. *International Journal of Applied Earth Observation and Geoinformation*, 112, 102866. doi.org/10.1016/j.jag.2022.102866

Rouse, J., Haas, R.H., Schell, J.A., Deering, D., 1973. Monitoring vegetation systems in the great plains with ERTS.

Song, C., Woodcock, C.E., Seto, K.C., Lenney, M.P., Macomber, S.A., 2001. Classification and Change Detection Using Landsat TM Data: When and How to Correct Atmospheric Effects? *Remote Sensing of Environment*, 75, 230–244. doi.org/10.1016/S0034-4257(00)00169-3.

Sriwongsitanon, N., Gao, H., Savenije, H. H. G., Maekan, E., Saengsawan, S., Thianpopirug, S., 2015. The Normalized Difference Infrared Index (NDII) as a proxy for soil moisture storage in hydrological modelling. *Hydrology and Earth System Sciences*, 12, 8419–8457. doi.org/0.5194/hessd-12-8419-2015

Struhár, J., Rapant, P., Kačmařík, M., Hlaváčová, I., Lazecký, M., 2022. Monitoring Non-Linear Ground Motion above

Underground Gas Storage Using GNSS and PSInSAR Based on Sentinel-1 Data. *Remote Sensing*, 14 4898. doi.org/10.3390/rs14194898.

Tarkowski, R., Lankof, L., Luboń, K., Michalski, J., 2024. Hydrogen storage capacity of salt caverns and deep aquifers versus demand for hydrogen storage: A case study of Poland. *Applied Energy*, 355, 122268. doi.org/ 10.1016/j.apenergy2023. 122268.

Yang X., Chen Y., Wang J., 2020. Combined use of Sentinel-2 and Landsat 8 to monitor water surface area dynamics using Google Earth Engine. *Remote Sensing Letters*, 11, 687–696. doi.org/10.1080/2150704X.2020.1757780

Zhang, T., Zhang, W., Yang, R., Gao, H., Cao, D., 2022. Analysis of Available Conditions for InSAR Surface Deformation Monitoring in CCS Projects, *Energies*, 15, 672. doi.org/10.3390/en15020672.